$Fe_3O_4/BaTiO_3$ COMPOSITES WITH CORE-SHELL STRUCTURE

Eugenia TANASĂ[1], Ecaterina ANDRONESCU[1*], Marin CERNEA[2], Ovidiu Cristian OPREA[1]

This paper demonstrates the possibility of the preparation of $Fe_3O_4/BaTiO_3$ core–shell composites. $BaTiO_3$-coated Fe_3O_4 ($Fe_3O_4/BaTiO_3$) with 5-15 nm Fe_3O_4 nanoparticles as cores and 2.5–4 nm $BaTiO_3$ shell thickness, was successfully prepared through coprecipitation method and sol-gel deposition technique. High-Resolution Transmission Electron Microscopy (HRTEM), Energy Dispersive X-ray Spectrometry (EDXS) and Selected-Area Electron Diffraction (SAED) showed the formation of the core–shell structure with face centered cubic Fe_3O_4 and tetragonal $BaTiO_3$ phases.

Keywords: Magnetite (Fe_3O_4) nanoparticles; Barium titanate ($BaTiO_3$); Coprecipitation; Sol–gel; Core–shell nanopowder

1. Introduction

In the last years, the core–shell nanomaterials have become a research field of great interest due to their potential applications in various fields, like: catalysts, sensors, electronics, optoelectronics and biomedical applications [1,2]. The composite materials consisting of components with distinct properties have also attracted attention due of their potential multifunctional applications [3,4]. Magnetite (Fe_3O_4) is the oldest magnetic material known. Magnetite nanoparticles have applications in magnetic bio-separation [5-7], drug delivery [8,9], magnetic resonance imaging contrast enhancement [10] and targeted drug [11-14], due to its excellent properties of superparamagnetism, biocompatibility, and low toxicity. However, pure magnetite nanoparticles may not be very useful in practical applications, since they are likely to form a large aggregation, alter magnetic properties, and undergo rapid biodegradation when they are directly exposed to the biological system. Therefore, for preventing such limitations from occurring, it is essential to coat the magnetite nanoparticles suitably [15]. Silica, polymer, $BaTiO_3$ and other are types of materials widely used in coating/modification of magnetite nanoparticles [16-18]. Barium titanate ($BaTiO_3$) is a typical dielectric material and is used extensively because of its high permittivity and unique ferroelectric, piezoelectric, and thermoelectric properties [19]. The core–shell

[1] Faculty of Applied Chemistry and Materials Science, University POLITEHNICA of Bucharest, Romania
[2] National Institute of Materials Physics, Bucharest-Magurele, Romania
[*]corresponding author: e-mail: ecaterina.andronescu@upb.ro

magnetic composites have shown great potential in bioseparation and functional immobilization [20,21]. In the $Fe_3O_4/BaTiO_3$ composite nanoparticle, Fe_3O_4 will act as an internal electrode for $BaTiO_3$ and, the composite nanoparticle will have high electromagnetic compatibility [22]. However, it is difficult to prepare the $Fe_3O_4/BaTiO_3$ heterostructure as a magnetic composite, due to partial oxidation of Fe_3O_4 to Fe_2O_3 in the calcination process for the preparation of $Fe_3O_4/BaTiO_3$ composite core-shell. In this paper, the co-precipitation method was used for the synthesis of Fe_3O_4 nanopowder and the sol-gel technique in order to cover the Fe_3O_4 particles with a $BaTiO_3$ layer/shell.

2. Materials and methods

2.1. Synthesis of $Fe_3O_4/BaTiO_3$ core-shell

Magnetite (Fe_3O_4) was prepared by co-precipitation method starting from iron(III) chloride ($FeCl_3$, 98%), heptahydrate iron sulfate ($FeSO_4 \cdot 7H_2O$, >99.0%) and ammonium hydroxide (NH_4OH). All reagents are provided by Sigma–Aldrich. The ferric chloride was dissolved in water at room temperature to give a clear solution. Iron sulfate is added to the solution as-obtained (Fe^{2+}/Fe^{3+}=1:2 molar ratio), at room temperature, under magnetic stirring and then, this solution is added to ammonium hydroxide and finally, Fe_3O_4 precipitates. The precipitate is separated from the solution using a strong magnet and washed several times with ethanol and distilled water until pH = 7. After washing, the Fe_3O_4 precipitate is dried in oven, at 60 ° C for 12 hours (Fig.1).

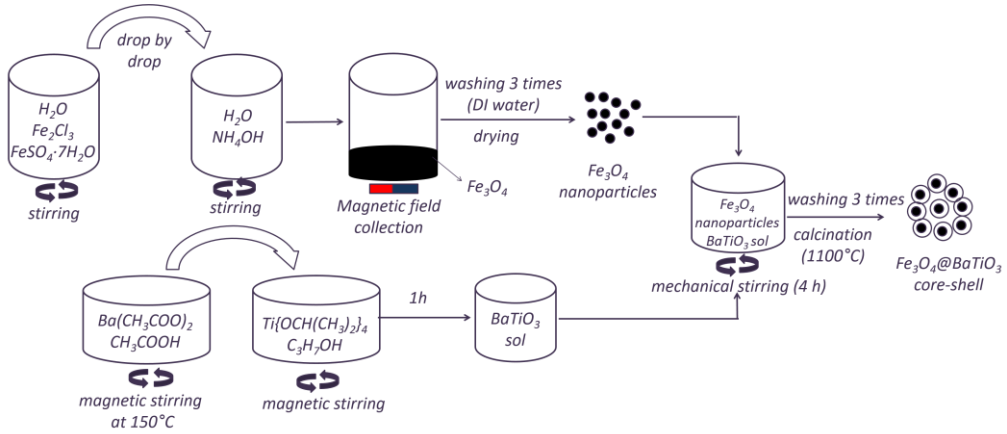

Fig.1. Schematic route for the synthesis of $Fe_3O_4/BaTiO_3$ core-shell

Barium titanate ($BaTiO_3$) was prepared by the sol-gel method using as starting reagents: barium acetate (Ba $(CH_3COO)_2$), titanium butoxide ($C_{16}H_{36}O_4Ti$), butyl alcohol, acetic acid and acetylacetone. All reagents of high purity are provided by Sigma–Aldrich. The barium acetate is dissolved in acetic acid. Titanium butoxide is added to butyl alcohol in order to obtain the optimal

concentration of the precursor sol that will cover the magnetite grains. By adding the acetic barium acetate solution to the titanium butoxide alcohol solution, the complex solution of Ba and Ti ($BaTiO_3$ precursor sol) is obtained. To stabilize the as-obtained sol, acetylacetone is added. The $Fe_3O_4/BaTiO_3$ core-shell composite results from the addition of $BaTiO_3$ sol to the magnetite powder of Fe_3O_4. For the sol surrounding the magnetite particles to turn into gel, the magnetite particles are kept in the sol suspension by mechanical agitation for several hours. Then, the magnetite granules coated with $BaTiO_3$ precursor gel are separated from the sol by centrifugation. Core-shell grains are washed several times with distilled water, dried at 70 °C and calcined at 700 °C for 1 hour, in argon with 10% hydrogen in order to crystallize $BaTiO_3$.

2.2. Characterization

The Fe_3O_4 and $Fe_3O_4/BaTiO_3$ core-shell dried precipitate and gel powders were analyzed by thermogravimetric (TG) and differential scanning calorimetry (DSC) methods using a Netzsch STA 449C Jupiter Instrument, at temperatures from 25 to 900 °C with a heating rate of 20 °C/min, in air atmosphere. The crystallographic structure of the core–shell composites was examined using a Panalytical X'Pert PRO MPD diffractometer. CuK_α radiation (wavelength 1.5406 Å) and Bragg–Brentano diffraction geometry were employed. X-ray diffraction data were acquired at room temperature with a step-scan interval of 0.02° and a step time of 40s. The microstructure of the core–shell heterostructures was assessed using a FEI QUANTA INSPECT F scanning electron microscope with field emission gun and a Tecnai^{TM} F30 G^2 S–TWIN transmission electron microscope with a line–resolution of 1.2 Å. The crystalline structure of the samples was investigated by selected area electron diffraction (SAED) and high resolution transmission electron microscopy (HRTEM). The local symmetry of the compounds was determined by Raman spectroscopy. Raman spectra were obtained at room temperature using a Horiba Jobin Yvon LabRAM HR800 spectrometer, equipped with nitrogen cooled detector. For excitation, the 632.8 nm He-Ne laser was employed for the characterization of the Fe_3O_4 nanoparticles and the 514 nm Argon Ion laser for the characterization of the $BaTiO_3$ and $Fe_3O_4/BaTiO_3$ compounds.

3. Results and discussion

3.1. Thermal analyses

Several thermal analyses (TG and DSC) were used for better distinction of the steps and the species that participate in the thermal transformations of the precipitate precursor of Fe_3O_4 and gel precursor of $BaTiO_3$ shell. The thermogravimetry curve recorded under air atmosphere, with 10 °C/min heating velocity, showed a gradual weight loss in the temperature range 25-900 °C for the precipitate.

According to major changes suggested by the shape of the TG and DSC (Fig.2) diagrams, the decomposition process can be divided into three steps: 25-180 °C, 180-400 °C and 400-900 °C. The first stage (below 180 °C) can be ascribed to the evaporation of absorbed water and ethanol on the grains surface, while the second stage beginning at about 180 °C is due to the removed of CO_2 absorbed on the grains surface. These processes correspond to the endothermic peaks at 160 °C and 220 °C on the DSC curve (Fig.2).

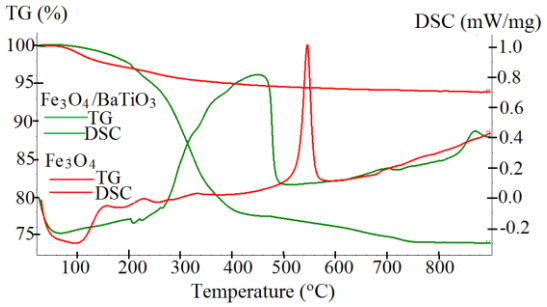

Fig.2. Thermal analyses (TG and DSC) results of Fe_3O_4 precipitate and $Fe_3O_4/BaTiO_3$ dried composite core-shell

The peak at 550 °C is probably due to the crystallization of the Fe_3O_4 phase. According to TG curve of $BaTiO_3$ shell gel in the temperature range of 25–900 °C, there are two steps (25-400 °C and 400-750 °C) of the thermal behavior of $BaTiO_3$ precursor gel. In the first range, butyl alcohol, acetic acid and acetylacetone evaporate. The loss of mass in the 400-750 °C range is due to the pyrolysis of the butoxide, acetate and acetylacetonate groups bonded to Ti and crystallization of $BaTiO_3$ phase.

3.2. XRD analyses

Fig. 3 shows the XRD patterns of the Fe_3O_4 powder used as core in the composite core-shell, $Fe_3O_4/BaTiO_3$ core-shell powder where the $BaTiO_3$ shell is a dried gel and, $Fe_3O_4/BaTiO_3$ calcined core-shell powder.

The diffraction peaks at 18.39°, 30.07°, 35.50°, 43.13°, 53.71°, 57.19°, and 62.69° were indexed as crystalline planes of (111), (220), (311), (400), (422), (511), and (440), respectively, for cubic spinel-like structural Fe_3O_4 (ICDD file no. 04-008-8147, space group: Fd-3m) [23]. As can be seen in Fig.3(b), the diffraction peaks were attributed to the face centered cubic Fe_3O_4 phase of the core particles and, some non-indexed peaks are assigned to the precursor gel of $BaTiO_3$. Fig. 3(c) shows peaks corresponding to face centered cubic Fe_3O_4, tetragonal $BaTiO_3$ (ICDD file no. 04-007-9921, space group: P4mm) [24] and, monoclinic $BaTi_5O_{11}$ phases (ICDD file no. 00-035-0805, space group: P21/n) [25] present as traces.

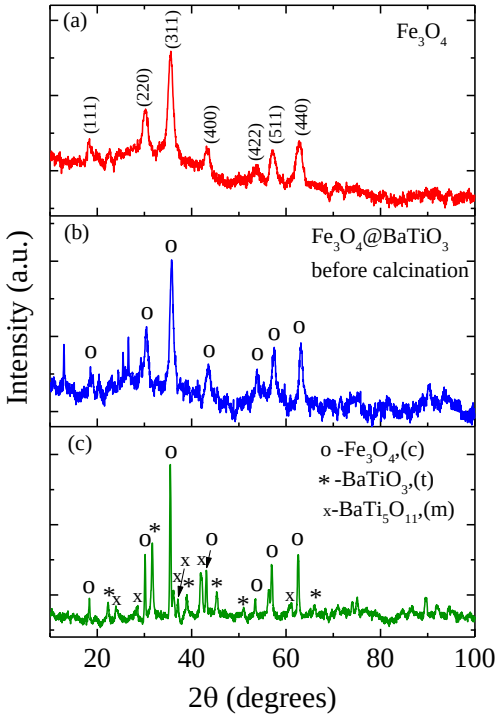

Fig.3. X-ray diffractograms: (a) magnetite powder obtained by coprecipitation; (b) $Fe_3O_4/BaTiO_3$ core-shell powder as-prepared; (c) $Fe_3O_4/BaTiO_3$ calcined core-shell powder

3.3. Raman analyses

The characteristic peaks positions of magnetite (Fe_3O_4) and $BaTiO_3$ determined in the Raman region of 100–900 cm^{-1} are presented in Fig.4.

The room-temperature Raman spectra of Fe_3O_4, $BaTiO_3$ and $Fe_3O_4/BaTiO_3$ composite (Fig.4), show a good comparative phonon assignment with other reports [26-29]. Thus, the bands at 193, 312, 545 and 671 cm^{-1} are attributed to Fe_3O_4, in good agreement with those previously reported [26-28]. For example, J. Dunnwald, A. Otto [27] reported bands at 298, 319, 418, 550, 676 cm^{-1} while, D.L.A. de Faria et al. [26], reported bands at 193 (week), 306 (week), 538 (week), 668 cm^{-1} (strong). The Raman spectrum for the $BaTiO_3$ powder sample obtained by us is presented in Fig.4(b). This spectrum shows peaks at: 261, 307, 516 and 718 cm^{-1}, that are close to those reported by others researchers [29]. The Raman mode around 303 cm^{-1} is characteristic of the tetragonal $BaTiO_3$; the other peaks can be attributed to both the cubic and tetragonal structure of $BaTiO_3$. Fig.4(c) shows the Raman spectrum of the $Fe_3O_4/BaTiO_3$ particles of core-shell biphasic composition. The Raman spectrum of the composite follows the spectrum of $BaTiO_3$ shell and the peaks of the core-shell are shifted vs. Fe_3O_4 peaks.

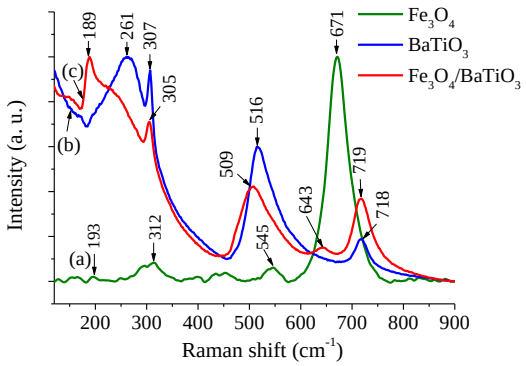

Fig.4. Raman spectra of (a) magnetite (Fe_3O_4) powder, (b) $BaTiO_3$ powder and (c) $Fe_3O_4/BaTiO_3$ calcined core-shell powder

3.4. SEM analysis

SEM micrographs of the Fe_3O_4 and $Fe_3O_4/BaTiO_3$ powders are shown in Fig.5.

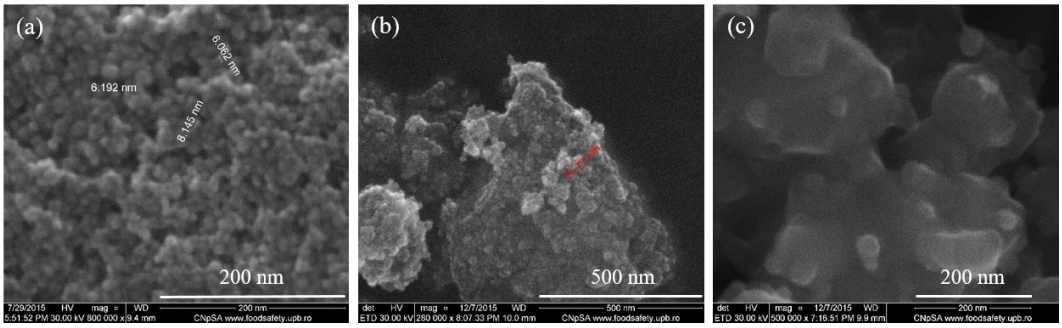

Fig.5. SEM micrographs of (a) Fe_3O_4 powder prepared by coprecipitation method, (b) $Fe_3O_4/BaTiO_3$ powder, after drying the $BaTiO_3$ shell gel, and (c) $Fe_3O_4/BaTiO_3$ powder, calcined at 700°C

Both powders present nano-sized grains. The Fe_3O_4 powder exhibit particles of 7 nm average size and agglomerates (Fig.5(a)). $Fe_3O_4/BaTiO_3$ powder, after drying the $BaTiO_3$ shell gel shows also agglomerates consisting of primary nanosized particles (~12 nm) (Fig.5(b)). The $Fe_3O_4/BaTiO_3$ core-shell powder, calcined at 700 °C show a structure composite with 0-3 connectivity (Fig. 5(c)).

3.5. TEM analysis

The size of nanoparticles and microstructure of the Fe_3O_4 powder are also studied using TEM and the results are shown in Fig.6.

The bright field transmission electron microscopy (BF-TEM) (Fig.6(a,b)) and high-resolution transmission electron microscopy (HR-TEM) images (Fig.6(c)) reveal that the average size of Fe_3O_4 are of about 6 nm. The inset of

indexed selected area electron diffraction (SAED) pattern (Fig.6(a)) shows that the powder is nanocrystalline (ring patterns). The measured interplanar distances are attributed to the face centered Fe_3O_4 compound (ICDD file no. 04-008-8147). This crystalline structure is validated by the HRTEM image (Fig.6(c)), where is highlighted the 2.53 Å interplanar distance of crystalline family planes with (311) Miller indices of face centered cubic Fe_3O_4. Fig.7 and Fig.8 demonstrate the core-shell architecture of the composite $Fe_3O_4/BaTiO_3$.

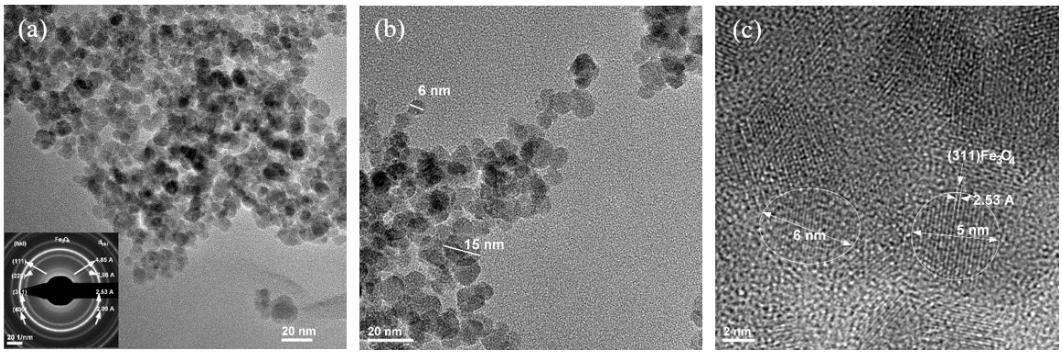

Fig.6. (a,b) TEM and (c) HR-TEM micrographs of (a) Fe_3O_4 powder prepared by coprecipitation method. (a) Inset of the selected-area electron diffraction (SAED) pattern for the Fe_3O_4 powder

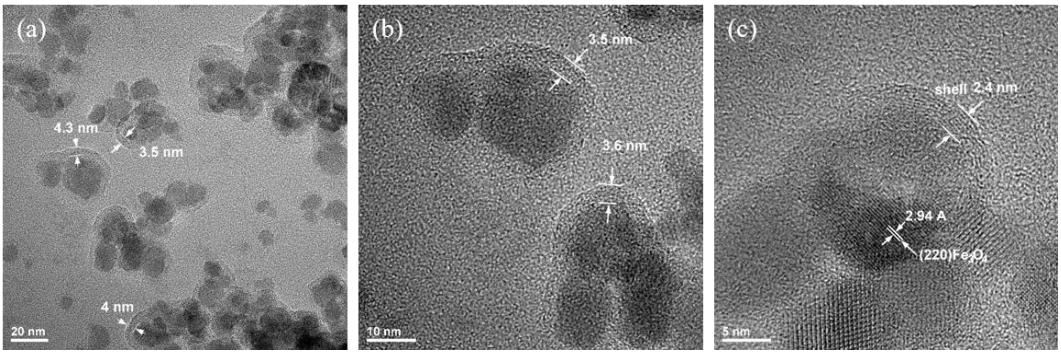

Fig.7. (a-c) TEM micrographs of $Fe_3O_4/BaTiO_3$ core-shell not calcined powder

As can be seen in Fig.7, the size of the $BaTiO_3$ shell is 2.5-4 nm. HR-TEM investigation indicated that the core is face centered cubic phase Fe_3O_4. The fringes spacing of 2.94 Å correspond to the interplanar spacing of crystalline family planes with (220) Miller indices of Fe_3O_4 phase (Fig.6(c)) [23].

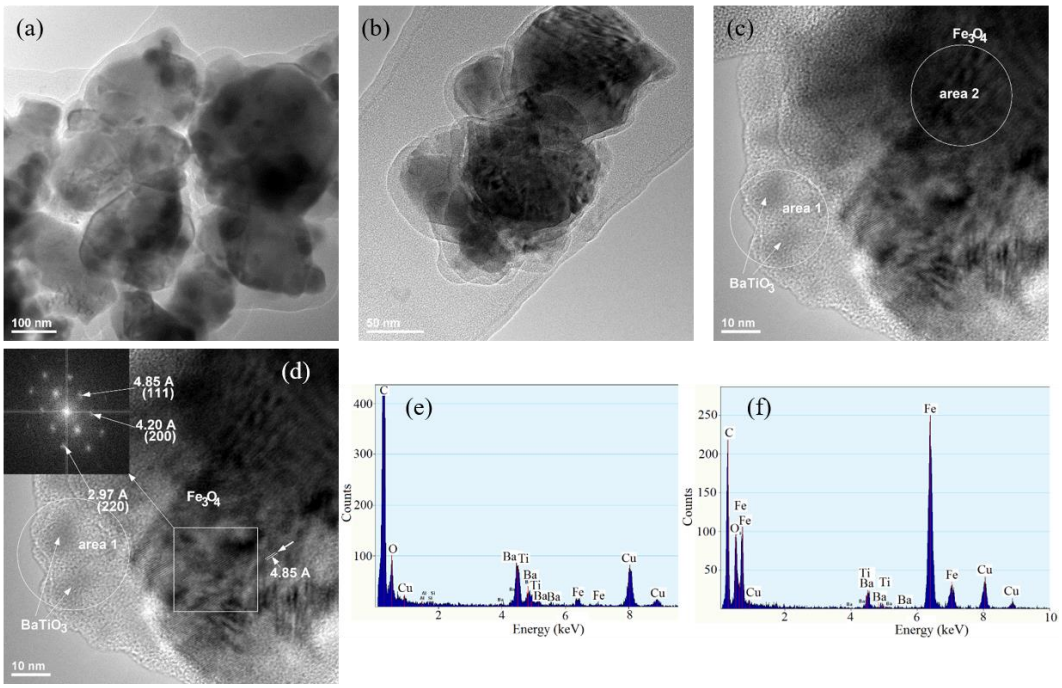

Fig.8. (a,b) TEM bright-field (BF) and (c,d) HR-TEM micrographs of $Fe_3O_4/BaTiO_3$ core-shell calcined powder at 700 °C for 1 hour, in argon with 10% hydrogen; (e, f) Energy Dispersive X-ray spectra (EDX) for $BaTiO_3$ and Fe_3O_4 acquired on highlighted area 1 and area 2, respectively

In Fig.8(c,d), two areas (area 1 and area 2) are highlighted, where $BaTiO_3$ and Fe_3O_4 phases are identified, respectively. EDX spectrum from Fig.8(e) shows the presence of major elements Ba and Ti in area 1, where the $BaTiO_3$ phase is predominant. In area 2, the major phase is Fe_3O_4, Fe being the major element (EDX spectrum from Fig.8(f)). The inset in Fig.8(d) is the Fast Fourier Transform (FFT) of the highlighted square area. The measurements of interplanar distances on the FFT shows the presence of the Fe_3O_4 phase.

4. Conclusions

In summary, the composite $Fe_3O_4/BaTiO_3$ core-shell was successfully prepared, using coprecipitation technique and sol–gel chemistry. XRD, Raman, SEM, TEM, HRTEM and SAED investigation demonstrated the core–shell structure of this composite. These methods indicated also that our composite core-shell show two main crystallographic phases (cubic Fe_3O_4 and tetragonal $BaTiO_3$) and traces of $BaTi_5O_{11}$ phase. SEM and TEM analyses shown both nano-sized particles of Fe_3O_4 and nanocomposite $Fe_3O_4/BaTiO_3$ powder.

From the references presented below, the research can be directed towards the possibility of the preparation of $Fe_3O_4/BaTiO_3$ core-shell material for biomedical applications.

Acknowledgement

The SEM and Raman spectroscopy characterizations were possible due to the Project POSCCE, No.638/12.03.2014.

R E F E R E N C E S

[1] *Campbell CT, Parker SC, Starr DE.* The effect of size–dependent nanoparticle energetics on catalyst sintering. Science **298,** (2002), 811–814.

[2] *Tsao HN, Cho D, Andreasenetal JW.* The influence of morphology on high–performance polymer field–effect transistors. Adv Mater **21,** (2009), 209–2012.

[3] *Zhang L, Zhai J, Mo W, Yao X.* The dielectric and leakage current behavior of $CoFe_2O_4$–$BaTiO_3$ composite films prepared by combining method of sol–gel and electrophoretic deposition. Solid State Sci **12,** (2010), 509–514.

[4] *Tan SY, Shannigrahi SR, Tan SH, Tay FEH*. Synthesis and characterization of composite $MgFe_2O_4$–$BaTiO_3$ multiferroic system. J Appl Phys **103,** (2008), 094105–4.

[5] *Park HY, Schadt MJ, Lim IIS, Kim SH, Jang MY, Luo J, Zhong CJ*. Fabrication of magnetic core@ shell Fe oxide@Au nanoparticles for interfacial bioactivity and bio-separation. Langmuir **23,** (2007), 9050–9056.

[6] *Long MJ, Pan Y, Lin HC, Hedstrom L, Xu B*. Cell compatible trimethoprim-decorated iron oxide nanoparticles bind dihydrofolate reductase for magnetically modulating focal adhesion of mammalian cells. J Am Chem Soc **133,** (2011), 10006–10009.

[7] *Pan Y, Du X, Zhao F, Xu B*. Magnetic nanoparticles for the manipulation of proteins and cells. Chem Soc Rev **41,** (2012), 2912–2942,

[8] *Kim J, Kim HS, Lee N, Kim T, Kim H, Yu T, Hyeon T*. Multifunctional uniform nanoparticles composed of a magnetite nanocrystal core and a mesoporous silica shell for magnetic resonance and fluorescence imaging and for drug delivery. Angew Chem Int Ed **47,** (2008), 8438–8441,

[9] *Luo Z, Cai KY, Hu Y, Li JH, Ding XW, Zhang BL, Xu DW*. Redox-responsive molecular nanoreservoirs for controlled intracellular anticancer drug delivery based on magnetic nanoparticles. Adv Mater **24,** (2012), 431–435.

[10] *Wang LY, Bao J, Wang L, Zhang F, Li YD*. One-pot synthesis and bioapplication of amine-functionalized magnetite nanoparticles and hollow nanospheres. Chem Eur J **12,** (2006), 6341–6347.

[11] *Pankhurst QA, Connolly J, Jones SK, Dobson J*. Applications of magnetic nanoparticles in biomedicine. J Phys D **36,** (2003), R167–R181.

[12] *Zhang J, Misra RDK*. Magnetic drug-targeting carrier encapsulated with thermosensitive smart polymer: core–shell nanoparticle carrier and drug release response. Acta Biomater **3,** (2007), 838–850.

[13] *Zhang L, Qiao SZ, Jin YG, Chen ZG, Gu HC, Lu GQ*. Magnetic hollow spheres of periodic mesoporous organosilica and Fe_3O_4 nanocrystals: fabrication and structure control. Adv Mater **20,** (2008), 805–809.

[14] *Zhang J, Rana S, Srivastava RS, Misra RDK*. On the chemical synthesis and drug delivery response of folate receptor-activated, polyethylene glycol-functionalized magnetite nanoparticles. Acta Biomater **4,** (2008), 40–48.

[15] *Yang Y, Guo X, Wei K, Wang L, Yang D, Lai L, Cheng M, Liu Q*. Synthesis and drug-loading properties of folic acid-modified superparamagnetic Fe_3O_4 hollow microsphere core/mesoporous SiO_2 shell composite particles, J Nanopart Res **16,** (2014,) 2210.
[16] *Deng Y, Qi D, Deng C, Zhang X, Zhao D*. Superparamagnetic high-magnetization microspheres with an Fe_3O_4@SiO_2 core and perpendicularly aligned mesoporous SiO_2 shell for removal of microcystins. J Am Chem Soc **130,** (2008), 28–29.
[17] *Szpak A, Kania G, Skorka T, Tokarz W, Zapotoczny S, Nowakowska M*. Stable aqueous dispersion of superparamagnetic iron oxide nanoparticles protected by charged chitosan derivatives. J Nanopart Res **15,** (2013), 1372.
[18] *Li X, Wang G, Cheng Y*. Preparation and characteristics of Fe_3O_4-$BaTiO_3$ heterostructural nanocomposite as photocatalyst. Res Chem Intermed **41,** (2015), 3031–3039.
[19] *Barsoum MW*. Fundamentals of Ceramics, McGraw–Hill, Boston, 1997.
[20] *Xu XQ, Deng CH, Gao MX, Yu WJ, Yang PY, Zhang XM*. Adv Mater **18,** (2006), 3289–3329.
[21] *Li Y, Yan B, Deng CH, Yu WJ, Xu XQ, Yang PY, Zhang XM*. Proteomics **7,** (2007) 2330–2339.
[22] *Adachi T, Wakiya N, Sakamoto N, Sakurai O, Shinozaki K, Suzuki H*. Spray Pyrolysis of Fe_3O_4–$BaTiO_3$ Composite Particles. J Am Ceram Soc. **92,** (2009) S177–S180.
[23] *Coker VS, Bell AMT, Pearce CI, Pattrick RAD, van der Laan G, Lloyd JR*. Am Mineral. **93,** (2008) 540.
[24] *Verbitskaya TN, Zhdanov GS, Venentsev IN, Soloviev SP*. Sov Phys Crystallogr (Engl. Transl.) **3,** (1958), 182.
[25] *Tillmanns von E*. Acta Crystallogr Sec B: Struct Crystallogr Cryst Chem. **25,** (1969), 1444.
[26] *de Faria DLA, Venancio Silva S, de Oliveira MT.* Raman Microspectroscopy of Some Iron Oxides and Oxyhydroxides. J Raman Spectrosc **28,** (1997), 873–878.
[27] *Dunnwald J, Otto A.* An investigation of phase transitions in rust layers using Raman spectroscopy. Corros Sci **29,** (1989), 1167-1176.
[28] *Slavov L, Abrashev MV, Merodiiska T, Gelev Ch, Vandenberghe RE, Markova-Deneva I, Nedkov I*. Raman spectroscopy investigation of magnetite nanoparticles in ferrofluids. J Magn Magn Mater **322**, (2010), 1904–1911.
[29] *Lazarevic Z, Romcevi N, Vijatovic M, Paunovic N, Romcevi M, Stojanovic B, Dohcevi-Mitrovi Z.* Characterization of Barium Titanate Ceramic Powders by Raman Spectroscopy. Acta Phys Pol A, **115,** (2009), 808-810.